

# The $s$ -process branching at $^{185}\text{W}$

K. Sonnabend, P. Mohr, K. Vogt, and A. Zilges  
*Institut für Kernphysik, Technische Universität Darmstadt,  
Schlossgartenstraße 9, D-64289 Darmstadt, Germany*

A. Mengoni  
*ENEA, V.le G. B. Ercolani 8,  
I-40138 Bologna, Italy*

T. Rauscher  
*Institut für Physik, Universität Basel,  
Klingelbergstrasse 82, CH-4056 Basel, Switzerland*

H. Beer and F. Käppeler  
*Forschungszentrum Karlsruhe, Institut für Kernphysik,  
P.O. Box 3640, D-76021 Karlsruhe, Germany*  
and

R. Gallino<sup>1</sup>  
*Dipartimento di Fisica Generale, Università di Torino  
and Sezione INFN di Torino, Via P. Giuria 1, I-10125 Torino, Italy*

## ABSTRACT

The neutron capture cross section of the unstable nucleus  $^{185}\text{W}$  has been derived from experimental photoactivation data of the inverse reaction  $^{186}\text{W}(\gamma, n)^{185}\text{W}$ . The new result of  $\sigma = (687 \pm 110) \text{ mbarn}$  confirms the theoretically predicted neutron capture cross section of  $^{185}\text{W}$  of  $\sigma \approx 700 \text{ mbarn}$  at  $kT = 30 \text{ keV}$ . A neutron density in the classical  $s$ -process of  $n_n = (3.8_{-0.8}^{+0.9}) \times 10^8 \text{ cm}^{-3}$  is derived from the new data for the  $^{185}\text{W}$  branching. In a stellar  $s$ -process model one finds a significant overproduction of the residual  $s$ -only nucleus  $^{186}\text{Os}$ .

*Subject headings:* nuclear reactions, nucleosynthesis, abundances

## 1. Introduction

The unstable nucleus  $^{185}\text{W}$  is a so-called branching point in the slow neutron capture process ( $s$ -process). The nucleus  $^{185}\text{W}$  is produced by neutron capture in the  $s$ -process from the stable

$^{184}\text{W}$ . At small neutron densities  $^{185}\text{W}$   $\beta$ -decays to  $^{185}\text{Re}$  with a half-life of  $T_{1/2} = 75.1 \text{ d}$ , and it has been pointed out that the  $\beta$ -decay half-life does practically not depend on the temperature at typical  $s$ -process conditions (Takahashi & Yokoi 1987). At higher neutron densities  $^{185}\text{W}$  may capture one more neutron leading to the stable  $^{186}\text{W}$ . It is obvious that the branching between  $\beta$ -decay and neutron capture depends on the  $\beta$ -decay half-

---

<sup>1</sup>temporary address: Max-Planck-Institut für Chemie, Abteilung Kosmochemie, Becherweg 27, D-55128 Mainz, Germany

life, the neutron capture cross section, and the neutron density. The half-life and the neutron capture cross section can be measured in the laboratory, and therefore one can determine the neutron density from the observed abundances of the various tungsten isotopes (Käppeler et al. 1991). Additionally, this branching has minor influence on the  $^{187}\text{Os}/^{187}\text{Re}$  cosmochronometer (Bosch et al. 1996).

Up to now, only theoretical estimates are available for the neutron capture cross section of  $^{185}\text{W}$  because direct neutron capture experiments with radioactive targets are very difficult. Theoretical predictions for the Maxwellian averaged capture cross section at a typical temperature of 30 keV vary significantly from 532 mbarn (Käppeler et al. 1991) and 560 mbarn (Rauscher & Thielemann 2000) to 794 mbarn (Holmes et al. 1976). In a recent compilation a value of  $(703 \pm 113)$  mbarn has been adopted (Bao et al. 2000). All calculations used the statistical model. The differences in the results come from the parameterizations of the level density, the gamma-ray strength function, and the neutron-nucleus optical potential.

In order to reduce the uncertainties, a new experiment was performed on the inverse reaction  $^{186}\text{W}(\gamma, n)^{185}\text{W}$ . The idea is to find a parameter set for the calculations which reproduces the cross section of  $^{186}\text{W}(\gamma, n)^{185}\text{W}$ , and to apply these parameters for the prediction of the  $^{185}\text{W}(n, \gamma)^{186}\text{W}$  cross section. Such a prediction should be more reliable for one special reaction than previous calculations which used global or local systematics to derive the relevant parameters from neighboring nuclei. The relevant energy region is located close above the threshold of the  $(\gamma, n)$  reaction at  $S_n = 7194$  keV (Mohr et al. 2001). At higher energies experimental data on the  $^{186}\text{W}(\gamma, n)^{185}\text{W}$  reaction are available in literature (Berman et al. 1969; Goryachev & Zalesnyĭ 1978; Gurevich et al. 1981), and the results can be found in the compilations of Dietrich & Berman (1988) and in CDFE (Varlamow et al. 2001). We have performed an additional measurement at energies close above the threshold.

In §2 we present our experimental set-up. In §3 we calculate the cross sections of the  $(n, \gamma)$  and  $(\gamma, n)$  reactions, in §4 we derive the  $s$ -process neutron density from our experimental data, and we apply a stellar  $s$ -process model to the  $^{185}\text{W}$

branching. §5 gives a summary and conclusions.

## 2. Experimental Set-up and Procedure

The  $^{186}\text{W}(\gamma, n)^{185}\text{W}$  experiment was performed using the photoactivation technique at the real photon set-up at the superconducting linear electron accelerator S-DALINAC (Richter 1996). Recently, several photoactivation experiments have been performed here (Mohr et al. 2000a; Vogt et al. 2001; Lindenberg et al. 2001; Mohr et al. 2000b), and  $(\gamma, n)$  cross sections and reaction rates were determined using a quasi-thermal photon bath at temperatures of several  $10^9$  K. These data are relevant for the nucleosynthesis of the neutron-deficient so-called  $p$ -nuclei (Lambert 1992).

Photons were generated by bremsstrahlung using our electron beam at an energy of  $E_0 = 8775$  keV and with a beam current of about  $30 \mu\text{A}$ . Usually, the photon beam is collimated and hits the target at a distance  $d_2 \approx 150$  cm behind the radiator target. This leads to a well-defined photon beam with a spectral composition which was analyzed in detail (Vogt et al. 2001). However, because of the relatively long half-life of  $^{185}\text{W}$  ( $T_{1/2} = (75.1 \pm 0.3)$  days) and the weak  $\gamma$ -ray branch ( $E_\gamma = 125.4$  keV) in the  $\beta$ -decay of  $^{185}\text{W}$  to  $^{185}\text{Re}$  of only  $(1.92 \pm 0.07) \times 10^{-4}$  (Kempisty & Pochwalski 1992) the irradiation of  $^{186}\text{W}$  had to be performed with the highest photon flux that can be obtained at our irradiation set-up. Therefore, the tungsten target was mounted directly behind the radiator target ( $d_1 \approx 5$  cm) where the photon intensity is roughly a factor of 300 higher than at our usual irradiation position. Fig. 1 shows an overview of our experimental setup. The target consisted of a thin metallic tungsten disk of natural isotopic composition with a diameter of  $\varnothing = 20$  mm and a thickness of about 1.2 mm. Note that the amount of target material remains limited because of the absorption of the low-energy decay  $\gamma$ -ray in the target. Properties of the target are summarized in Table 1. The decay properties of the residual nuclei are listed in Table 2.

To minimize systematic uncertainties from the photon flux determination at the position directly behind the radiator target, a relative measurement was carried out. We irradiated simultaneously the tungsten target and a very thin ( $25 \mu\text{m}$ ) gold disk at the position close to the radiator tar-

get. A second thin gold disk was sandwiched between two layers of boron. This sandwich target was mounted at the regular target position and irradiated simultaneously with the tungsten and gold targets close to the radiator. The boron target is used to normalize the incoming photon intensity by the  $^{11}\text{B}(\gamma, \gamma')$  reaction. From the absolute photon intensity at the regular target position and from the activation of the second thin gold target one can determine the  $(\gamma, n)$  cross section of  $^{197}\text{Au}$ . The complete determination of the  $^{197}\text{Au}(\gamma, n)^{196}\text{Au}$  cross section is presented in Vogt et al. (2002). And, finally, the  $^{186}\text{W}(\gamma, n)$  cross section can be determined from the ratios of activities of the gold and tungsten targets close to the radiator. Absorption of bremsstrahlung  $\gamma$ -rays in the targets can be neglected. Typical uncertainties for the photon flux determination are of the order of 10%. Further details of the experimental set-up can be found in Vogt et al. (2001) and Mohr et al. (1999).

The decay  $\gamma$ -rays of the activated tungsten and gold targets were measured using a well-shielded high-purity germanium (HPGe) detector with a relative efficiency of 30% and an energy resolution of 2 keV (at 1332.5 keV). A typical spectrum of the tungsten target is shown in Fig. 2. We followed the decay of the activity over more than one half-life, and the analysis of our decay curve leads to a half-life of  $T_{1/2} = (76.6 \pm 1.5) \text{ d}$  which agrees with the adopted value of  $T_{1/2} = (75.1 \pm 0.3) \text{ d}$  (ENSDF 2001) within the uncertainties. The precise exponential decay of the activity confirms that the analyzed  $\gamma$ -ray line does not accidentally overlap with a background line. Of course, also the excellent energy resolution of the HPGe detector helps to measure a weak  $\gamma$ -ray branching. The efficiency of the HPGe detector was determined by calibrated sources (Vogt et al. 2001). Additionally, for the 125.4 keV  $\gamma$ -ray from the  $^{185}\text{W}$  decay the self-absorption in the tungsten target was taken into account by GEANT simulations (Brun & Carminati 1993), and the GEANT simulations of the absorption in tungsten were verified by transmission measurements of the tungsten target. The resulting uncertainty of the relative efficiency is about 5%.

The yield  $Y$  in our experiment is proportional

to the energy-integrated cross section  $I_\sigma$ :

$$Y \sim I_\sigma = \int_{S_n}^{E_0} N_{\text{br}}(E, E_0) \sigma(E) dE \quad (1)$$

with  $E_0$ : endpoint energy of the bremsstrahlung and kinetic energy of the electron beam;  $N_{\text{br}}(E, E_0)$ : number of bremsstrahlung photons at an energy  $E$  and with the endpoint energy  $E_0$ ;  $\sigma(E)$ :  $^{186}\text{W}(\gamma, n)^{185}\text{W}$  cross section. The factor between the yield  $Y$  and the energy-integrated cross section  $I_\sigma$  depends on characteristics of the observed isotope as well as on parameters of the experimental setup (Vogt et al. 2001). From the experimentally measured yield ratio  $Y_{\text{W}}/Y_{\text{Au}}$  between the tungsten and the gold yields one can derive the ratio of the integrated cross sections  $I_{\sigma, \text{W}}/I_{\sigma, \text{Au}} = 12.3 \pm 0.9$  with relatively small uncertainties. Note that the relatively large value of this ratio does not indicate that the cross section of  $^{186}\text{W}$  is much larger than the cross section of  $^{197}\text{Au}$ . The reason for this large ratio is the much smaller neutron separation energy  $S_n$  of  $^{186}\text{W}$  compared to  $^{197}\text{Au}$  which leads to a broader integration range in Eq. (1) for  $^{186}\text{W}$ .

It is not possible to determine the energy dependence of the  $^{186}\text{W}(\gamma, n)^{185}\text{W}$  cross section from one photoactivation measurement with a white bremsstrahlung spectrum. If one adopts the theoretically calculated energy dependence of the cross section  $\sigma(E)$  (see § 3), it is possible to solve the integral in Eq. (1) and to determine a normalization factor  $F$  for the theoretical calculation by comparison of the theoretically predicted and experimentally measured yields. In the case of the  $^{186}\text{W}(\gamma, n)^{185}\text{W}$  reaction this leads to normalization factors of  $F = Y_{\text{exp}}/Y_{\text{calc}}$  close to unity for two different calculations of the  $^{186}\text{W}(\gamma, n)^{185}\text{W}$  cross section (see § 3). The same factors  $F$  should be used for the prediction of the inverse  $^{185}\text{W}(n, \gamma)^{186}\text{W}$  cross section.

The reaction  $^{197}\text{Au}(\gamma, n)^{196}\text{Au}$  has been used to normalize the  $^{186}\text{W}(\gamma, n)^{185}\text{W}$  experiment. The determination of the  $^{197}\text{Au}(\gamma, n)^{196}\text{Au}$  cross section has been performed similar to Vogt et al. (2001) and is published elsewhere (Vogt et al. 2002). Our new data agree nicely with several previous experiments (Berman et al. 1987; Veyssi re et al. 1970) and a recent experiment with monochromatic photons from Laser-Compton backscattering (Utsunomiya 2001).

The experimental uncertainties are dominated (i) by the photon flux determination which enters into the analysis of the experimental yields in Eq. (1) for both the target  $^{186}\text{W}$  and the standard  $^{197}\text{Au}$ , and (ii) by the self-absorption of the 125.4 keV  $\gamma$ -ray in the tungsten target. The total uncertainty for the normalization factors  $F$  is 14 %.

The normalized calculations are compared with experimental data at higher energies in Figs. 3 and 4. Within the uncertainties one finds excellent agreement. Additionally, the dotted line shows the integrand of Eq. (1); this line defines the energy range where our experiment was sensitive. As a consequence of the white bremsstrahlung spectrum and the calculated energy dependence of the  $(\gamma, n)$  cross section, the energy range of our experiment is located directly above the  $(\gamma, n)$  reaction threshold, and it has a width of roughly 1 MeV. It is not possible to present our result as one data point in Figs. 3 and 4. Instead, the experimental result of this work are normalization factors  $F$  for the theoretical calculations.

### 3. Calculation of the $(\gamma, n)$ and $(n, \gamma)$ Cross Sections

Two sets of calculations, HF-1 and HF-2, of the relevant cross sections have been performed. In both cases the statistical model Hauser-Feshbach theory has been applied to describe the reaction process. Then, in one case, HF-1, a global set of parametrization was used, where the main model parameters were derived either from microscopic approaches or from global systematics. In the other case, HF-2, the model parameters were optimized to the mass region under consideration and, when possible, parameters derived from experimental nuclear structure data were used.

The calculation HF-1 was performed with the code NON-SMOKER (Rauscher & Thielemann 1998, 2000). The neutron transmission coefficients were computed using a microscopic potential (Jeukenne, Lejeune, & Mahaux 1977). Nuclear levels as given in Rauscher & Thielemann (2001) have been utilized. Above the last known state a global theoretical level density description was used (Rauscher, Thielemann, & Kratz 1997). The E1  $\gamma$ -transition probabilities were described by a Lorentzian shape with a modified low-

energy tail, following the prescription of McCullagh, Stelts, & Chrien (1981). Width and energy position of the GDR were also taken from theory. From a hydrodynamic droplet approach (Myers et al. 1977) we obtain  $E_{\text{GDR}} = 14.23$  MeV, and from a parameterized approach (Cowan, Thielemann, & Truran 1991) the width is determined as  $\Gamma_{\text{GDR}} = 5.45$  MeV. The modified energy-dependent width is then given as  $\Gamma(E_\gamma) = \Gamma_{\text{GDR}} \sqrt{E_\gamma/E_{\text{GDR}}}$ . For a deformed nucleus, the energy and width split according to the description outlined in Cowan, Thielemann, & Truran (1991). However, within the droplet model (Myers et al. 1977) the nucleus  $^{186}\text{W}$  is spherical and a single-humped Lorentzian with the above energy and width is obtained.

The calculation HF-2 was performed using the optical model parameters (OMP) of Moldauer (1965), for neutron transmission coefficients. This set of OMP reproduces fairly well the total cross sections of nuclei with  $A = 184$ -188. For example, the total cross section of  $^{186}\text{W}$  is reproduced with an accuracy of better than 10% for neutron energies from 100 keV up to 10 MeV, by this OMP set. Gamma-ray transmission coefficients were derived from the experimental double-humped GDR parameters (Dietrich & Berman 1988) derived from experimental  $(\gamma, n)$  data in the GDR region. The relevant data are:  $E_{\text{GDR}} = 12.59$  MeV and 14.88 MeV,  $\Gamma_{\text{GDR}} = 2.29$  MeV and 5.18 MeV, and  $\sigma_{\text{GDR}}^{\text{peak}} = 211$  mbarn and 334 mbarn, for the two GDR components. Nuclear level densities were derived from the parametrization of Mengoni & Nakajima (1994). Experimental discrete levels have been used to fit the constant-temperature parametrization at low excitation energies, matched to the pairing+shell corrected Fermi-gas model (Gilbert-Cameron prescriptions) at excitation energies close to the neutron binding energy.

In order to compare the results of model predictions with the present  $^{186}\text{W}(\gamma, n)^{185}\text{W}$  experimental data, the calculation of the cross sections for  $^{185}\text{W}$  in the ground state, as well as in several excited states have to be performed. Here, we have included excited states up to about 500 keV. Higher excited states do not appreciably contribute to the cross section. This request is altogether similar to what is needed to evaluate the  $(n, \gamma)$  cross section for thermally excited target states in stellar plasma (stellar cross sections).

From a comparison with the present experimental data close to the neutron threshold, a renormalization factor  $F_1 = 1.223$  is obtained for the global HF-1, and  $F_2 = 0.974$  for the local HF-2 calculation. Both calculations are able to reproduce the measured data from the neutron threshold up to the GDR region (see Figs. 3 and 4). The typical uncertainty of 25 to 30 % associated with neutron capture cross section calculations (see for example the prediction of the NON-SMOKER code (Rauscher, Thielemann, & Kratz 1997; Bao et al. 2000)) is therefore obtained with either model parameterizations.

It is interesting to note the similarity in the results of both calculations despite the strongly differing treatments of the GDR, which would be expected to dominate the difference in the results. Although HF-1 uses a single-humped GDR shape, a similar strength distribution as for HF-2 with its double-humped GDR is obtained at the low-energy side of the GDR. This is due to the use of an energy-dependent width, a slightly smaller GDR energy, and a slightly broader basic GDR width. Thus, the energy-dependence of the resulting cross section in the relevant energy range is almost the same for both calculations. The absolute values are roughly proportional to the  $\gamma$ -ray strength function, hence, they show a comparatively small difference.

The impact of other model inputs, such as the optical neutron potential, are rather small. When comparing the Maxwellian averaged cross sections obtained in the two descriptions, we notice increasing deviations at the lowest energies, i.e. below 10 keV. This means that a different energy dependence of the cross sections is found, being mainly due to the different optical model potentials used. At higher energies the energy dependence of the HF-1 and HF-2 calculations is similar and thus the uncertainties stemming from the optical potentials are not significant to explain further differences in the two approaches.

We will assume that the same renormalization factors derived from the present experimental data and model calculations, are valid also for the Maxwellian averaged cross section of the reverse reaction  $^{185}\text{W}(n,\gamma)^{186}\text{W}$ . This assumption requires some more discussion. What is actually measured and calculated here is a compound reaction in which the “compound” nucleus consists of

excited states of  $^{186}\text{W}$  created by  $\gamma$ -excitation of the ground state of  $^{186}\text{W}$ . This compound nucleus subsequently decays in the neutron channel to all energetically possible final states in  $^{185}\text{W}$ , according to the Bohr hypothesis, i.e. independently of how it was formed. For a full application of detailed balance linking the  $(n,\gamma)$  and  $(\gamma,n)$  reaction rates or Maxwellian averaged cross sections, one would have to use a Planck distribution of photons according to the astrophysical temperature of interest ( $\simeq 0.348 \times 10^9$  K) plus account for thermal excitation of the target at the same temperature instead of keeping the target in the ground state. Thus, for each photon energy we are actually measuring a subset of the transitions relevant for the capture rate. Applying detailed balance directly yields a neutron capture cross section which is the thermally averaged sum of neutron captures on the ground state and excited states of  $^{185}\text{W}$ , forming  $^{186}\text{W}$  at the given energy and finally directly decaying to the ground state of the final nucleus  $^{186}\text{W}$ . However, this cross section is governed by the same uncertainties in the optical neutron potential, the level densities, and the GDR properties as the full stellar cross section. Since the energy dependence of the  $(\gamma,n)$  reaction is well described by both models, it can safely be assumed that there is no further energy dependence in the renormalization factor. Therefore, we argue that the same renormalization factor can be applied also to the Maxwellian averaged cross section at 30 keV.

### 3.1. Results for $^{185}\text{W}(n,\gamma)^{186}\text{W}$

The normalized results of both calculations for the Maxwellian averaged cross section of  $^{185}\text{W}(n,\gamma)^{186}\text{W}$  at  $kT=30$  keV are in remarkable agreement: from HF-1 one obtains  $\sigma = 734$  mbarn, and from HF-2  $\sigma = 640$  mbarn. The average value is  $687 \text{ mbarn} \pm 100 \text{ mbarn}$  (experimental uncertainty)  $\pm 47 \text{ mbarn}$  from different calculations leading to a final result of  $(687 \pm 110) \text{ mbarn}$ . This value is already the stellar capture cross section at  $kT = 30$  keV where an enhancement factor of 0.92 was used; the cross section at  $kT \approx 0$  is  $747 \text{ mbarn}$  which is in agreement with the adopted value of  $(703 \pm 103) \text{ mbarn}$  (Bao et al. 2000) within the uncertainties. Contrary to this adopted value which was based on an empirical renormalization of a theoretical value, the new result is based on

experimental data of the inverse reaction. The compatibility of both values nicely confirms the estimate of the systematic error in the theoretical calculation which was used to generate the adopted value in Bao et al. (2000).

#### 4. The Branching at $^{185}\text{W}$

##### 4.1. The classical $s$ -process

The  $s$ -process synthesis path in the W-Re-Os mass region is shown in Fig. 5. The nuclei  $^{186,187}\text{Os}$  are partially bypassed by the  $s$ -process flow especially by a branching at  $^{185}\text{W}$ . The stellar beta decay rates of  $^{185}\text{W}$  and  $^{186}\text{Re}$  are practically independent of temperature in the relevant temperature region (Takahashi & Yokoi 1987). Therefore, the isotopic abundance of  $^{186}\text{Os}$  is determined by the average  $s$ -process neutron density. In Fig. 5 laboratory half-lives are indicated. However, according to Takahashi & Yokoi (1987), at stellar temperatures of interest the  $^{187}\text{Re}$  nucleus is almost fully ionized and its  $\beta^-$ -decay rate increases by about ten orders of magnitude ( $T_{1/2} = 21.3$  yr at a temperature  $T = 3 \times 10^8$  K and electron density  $n_e = 10$ ). In the same stellar environment,  $^{187}\text{Os}$ , which is stable in terrestrial conditions, becomes unstable by electron capture ( $T_{1/2} = 1243$  yr). Consequently, the abundance ratio between the two nuclei in the He intershell production zone and in the AGB envelope needs to be followed carefully.

The classical  $s$ -process model formulated by Ward, Newman, & Clayton (1976) provides a simple way of estimating the  $s$ -process neutron density via branching analyses. Previous analyses (Käppeler et al. 1991) of the W-Re-Os branching can now be updated with a neutron capture cross section for  $^{185}\text{W}$  which is not only based on statistical model calculations.

Except for our  $^{185}\text{W}$  capture cross section, the other relevant stellar cross for the  $s$ -process calculations were taken from the compilation of Bao et al. (2000). The  $s$ -process flow was normalized at the  $s$ -only isotope  $^{150}\text{Sm}$  which represents an accurate measure of the unbranched  $N\sigma$  curve and calculated down to the W-Re-Os branching using programs described by Beer, Corvi, & Mutti (1997) with an average exposure of  $\tau_0 = 0.296 (kT/30 \text{ keV})^{1/2} \text{ mbarn}^{-1}$ . This value corresponds also with a value reported by Ar-

landini et al. (1999). The relevant part of the calculation, the mass region from  $A = 145$  to the termination of the  $s$ -process at  $A = 209$  is shown in Fig. 6. In this part the overall feature of the  $N\sigma$  curve is a slow decrease up to  $A = 200$ . This mass region includes not only the studied W-Re-Os branching and the  $s$ -only  $^{150}\text{Sm}$  isotope on the unique synthesis path used for normalization of the  $N_s\sigma_s$  curve but also other important  $s$ -process branchings. These are first the branchings that are sensitive exclusively to the neutron density, i.e., the Nd-Pm-Sm ( $A = 147 - 150$ ), Er-Tm-Yb ( $A = 169 - 171$ ), W-Re-Os ( $A = 185 - 187$ ), and the Os-Ir-Pt ( $A = 191 - 193$ ) branchings, and second the branchings dependent on neutron density, temperature and electron density, i.e., the Sm-Eu-Gd ( $A = 151 - 152$ ), Eu-Gd ( $A = 154 - 156$ ), and Dy-Er ( $A = 163 - 164$ ) branchings. To adjust the  $s$ -process neutron density, temperature, and electron density, requires an  $s$ -only isotope to be located inside the branching. These empirical data points are shown in Fig. 6 as full solid circles with smaller  $N_s\sigma_s$  values than the  $N_s\sigma_s$  value of the unique synthesis path represented by  $N_s\sigma_s(^{150}\text{Sm})$ . For the W-Re-Os branching (Fig. 5) the branch point isotope is  $^{186}\text{Os}$ .

With the new stellar  $^{185}\text{W}$  cross section an average neutron density of

$$n_n = 3.8_{-0.8}^{+0.9} \times 10^8 \text{ cm}^{-3} \quad (2)$$

was found. The uncertainty of the  $^{185}\text{W}$  cross section contributes by  $(^{+16\%}_{-12\%})$ . The main uncertainty in the present  $n_n$  determination comes from the 6.3% uncertainty in the  $N\sigma$  value of  $^{186}\text{Os}$  which transforms to an error of  $(^{+23\%}_{-20\%})$  in the neutron density. The 6.3% uncertainty in  $N\sigma(^{186}\text{Os})$  is primarily the uncertainty of the solar osmium abundance (Anders & Grevesse 1989).

The present neutron density is still consistent with the Nd-Pm-Sm branching (Reifarth et al. 2002) but is too high for reproducing the Er-Tm-Yb and - in particular - Os-Ir-Pt branchings. While the parameters of the first case are rather uncertain, the Os-Ir-Pt branching has recently been studied with much improved cross sections yielding a neutron density of only  $0.7 \times 10^8 \text{ cm}^{-3}$  (Koehler et al. 2001). In Table 3 our present value for the neutron density is compared with corresponding results from other branchings.

The present neutron density in combination

with the adopted values for the  $s$ -process temperature of  $kT=27.1$  keV (Beer, Corvi, & Mutti 1997), and for the electron density of  $n_e = 5.4 \times 10^{26} \text{ cm}^{-3}$  (Arlandini et al. 1999) provides also to a fair reproduction of the other branchings shown (Fig. 5). The empirical  $N_s \sigma_s$  values of  $^{152}\text{Gd}$  and  $^{164}\text{Er}$  are underproduced in the calculation. This is reasonable as significant  $p$ -process contributions of up to 50 % and about 10 % can be expected for  $^{152}\text{Gd}$  and  $^{164}\text{Er}$ , respectively.

The discrepant neutron densities derived from different branchings as listed in Table 3 indicate an inherent difficulty of the classical model due to the rather schematic assumption of constant neutron density and temperature during the  $s$ -process. Hence, a consistent description of the various branchings has to be based on more realistic scenarios provided by stellar model calculations.

#### 4.2. The $s$ -process in AGB stars

The main component of the  $s$ -process nucleosynthesis occurs during helium shell burning in low mass AGB stars. The evolution of these stars and the related  $s$ -process nucleosynthesis has been discussed extensively by Gallino et al. (1998) and Busso et al. (2001), and it has been shown that this model is able to reproduce the main  $s$ -process component within 10 % (Arlandini et al. 1999) as the result of the average composition of the  $s$ -process abundance distribution of two AGB stellar models of  $1.5 M_\odot$  and  $3 M_\odot$  and a metallicity of  $Z = 0.01$ . In this model, the  $s$ -process is driven by two neutron sources. The first,  $^{13}\text{C}(\alpha, n)^{16}\text{O}$ , operates in the interpulse period between two helium flashes, and the second,  $^{22}\text{Ne}(\alpha, n)^{25}\text{Mg}$ , is activated at higher temperatures during the helium shell flash where almost the whole He intershell, i.e. the region between the H shell and the He shell, becomes convective for a relatively short period of time. The  $^{13}\text{C}$  neutron source accounts for about 95 % of the total neutron exposure in a thin radiative layer of about  $10^{-4} M_\odot$ ; however, the produced  $s$ -process abundances that depend on branching points along the  $s$ -path are significantly modified by the  $^{22}\text{Ne}$  source which is operating in the convective helium burning zone. After a limited number of helium shell flashes, at the quenching of the thermal instability, the convective envelope penetrates in the top region of the He intershell, dredging up  $^{12}\text{C}$  and  $s$ -process

rich material. The envelope is progressively lost by strong AGB winds and remixed into the interstellar medium.

It is important to emphasize that the profiles for neutron density and temperature are now provided by the stellar model. Therefore, the abundance patterns of  $s$ -process branchings represent a critical test for this stellar model.

The analysis of the branching at  $^{185}\text{W}$  shown in Fig. 5 leads to a significant overproduction of the  $s$ -only isotope  $^{186}\text{Os}$  by 20 % in this stellar  $s$ -process model. All neutron capture cross sections have been taken from the compilation of Bao et al. (2000) with the exception of the  $^{185}\text{W}(n, \gamma)^{186}\text{W}$  cross section where the present result was used. This means that the model apparently overestimates the  $\beta^-$ -decay part and/or underestimates the neutron capture part of the  $^{185}\text{W}$  branching. Consequently, it underestimates the  $s$ -process contribution to  $^{187}\text{Re}$ . Note that the uncertainties of the previously existing calculated  $^{185}\text{W}$  cross sections (Bao et al. 2000) were generous enough to allow for a roughly consistent description of the observed  $^{186}\text{Os}$  abundance.

The observed abundance of  $^{186}\text{Os}$  can be reproduced by the stellar model if one increases the  $^{185}\text{W}(n, \gamma)^{186}\text{W}$  cross section by 60 %. However, such an enhancement is outside the present experimental uncertainties. If the  $^{185}\text{W}(n, \gamma)^{186}\text{W}$  cross section is enhanced within the experimental uncertainties of about 20 %, one still finds an overproduction of  $^{186}\text{Os}$  by 12 % which is still slightly inconsistent with the observed abundance.

There are several possible explanations to cure this problem. First, the  $^{186}\text{Os}(n, \gamma)^{187}\text{Os}$  cross section could be 20 % larger than the adopted value by Bao et al. (2000). However, this value is based on two independent experiments who quote uncertainties between five and ten per cent (Winters & Macklin 1982; Browne & Berman 1981). Secondly, the additional branching at  $^{186}\text{Re}$  could reduce the  $^{186}\text{Os}$  abundance either by an increased  $^{186}\text{Re}(n, \gamma)^{187}\text{Re}$  cross section or by enhanced electron capture of  $^{186}\text{Re}$  under stellar conditions. However, it has been pointed out by Takahashi & Yokoi (1987) that under any realistic assumptions for the capture cross section and the ratio between  $\beta^-$ -decay and electron capture, the  $^{186}\text{Re}$   $\beta^-$ -decay is always faster than the neutron capture.

All these nuclear physics questions will be studied in additional experiments in the near future. Neutron capture experiments on osmium isotopes are planned at the new n\_TOF facility at CERN and at the Karlsruhe Van de Graaff accelerator, where uncertainties of the order of 1% can be achieved using the  $4\pi$  BaF<sub>2</sub> detector. Additionally, the  $^{187}\text{Re}(\gamma, n)^{186}\text{Re}$  cross section shall be measured using the monochromatic photon beam available from Laser-Compton backscattering at AIST, Tsukuba, thus allowing to improve the cross section for the inverse  $^{186}\text{Re}(n, \gamma)^{187}\text{Re}$  reaction.

With these improvements and by using a realistic *s*-process model there is a good chance for analyzing the  $^{185}\text{W}$  and  $^{186}\text{Re}$  branchings with sufficient confidence to establish the abundance of  $^{186}\text{Os}$  as a sensitive test for the stellar model.

## 5. Summary and Conclusions

We have measured the photodisintegration cross section of the  $^{186}\text{W}(\gamma, n)^{185}\text{W}$  reaction at energies near the reaction threshold. The experimental data have been used to restrict model predictions for the  $A = 186$  system and to derive the neutron capture cross section of the inverse  $^{185}\text{W}(n, \gamma)^{186}\text{W}$  reaction. The result of  $\sigma = (687 \pm 110)$  mbarn is close to the calculated cross section which was recommended by Bao et al. (2000), but exhibits significantly improved reliability.

The *s*-process flow at the branch point isotope  $^{185}\text{W}$  has been analyzed within the classical *s*-process model and within a realistic stellar model for AGB stars. With the classical model one obtains a neutron density of  $3.8 \times 10^8/\text{cm}^3$  compatible with the analyses of the branchings at  $A = 147/148$ , but incompatible with the branchings at  $A = 169/170$  and  $191/192$ . This inconsistency indicates that the assumptions of the classical model are too schematic to account for the stellar situation, where the *s* process takes place. The corresponding analysis based on a more realistic stellar model overestimates the  $^{186}\text{Os}$  abundance by 20%. Presently, we are facing the question whether this mismatch is related with remaining uncertainties in other nuclear physics data or whether it originates from the *s*-process model itself. If the nuclear physics uncertainties can be further reduced, the *s*-process branching at  $^{185}\text{W}$

can be interpreted as a sensitive test of models for the important AGB phase of stellar evolution.

We thank the S-DALINAC group around H.-D. Gräf for the stable beam during this activation experiment. Encouraging discussions with A. Richter and H. Utsunomiya are gratefully acknowledged. We thank the referee R. D. Hoffman for his encouraging report and helpful comments. This work was supported by the Deutsche Forschungsgemeinschaft (contracts Zi 510/2-1 and FOR 272/2-2) and by the Italian MURST-Cofin 2000 Project “Stellar Observables of Cosmological Relevance”.

## REFERENCES

- Anders, E. & Grevesse, N., 1989, *Geochim. Cosmochim. Acta*, 53, 197
- Arlandini, C., Käppeler, F., Wisshak, K., Gallino, R., Lugaro, M., Busso, M., & Straniero, O., 1999, *ApJ*, 525, 886
- Bao, Z. Y., Beer, H., Käppeler F., Voss, F., Wisshak, K., & Rauscher, T., 2000, *At. Data Nucl. Data Tables*, 76, 70
- Berman, B. L., Kelly, M. A., Bramblett, R. L., Caldwell, J. T., Davis, H. S., & Fultz, S. C., 1969, *Phys. Rev.*, 185, 1576
- Berman, B. L., Pywell, R. E., Dietrich, S. S., Thompson, M. N., McNeill, K. G., & Jury, J. W., 1987, *Phys. Rev. C*, 36, 1286
- Beer, H., Corvi, F., & Mutti, P., 1997, *ApJ*, 474, 843
- Bosch, F., et al., 1996, *Phys. Rev. Lett.*, 77, 5190
- Browne, J. & Berman, B., 1981, *Phys. Rev. C*, 23, 1434
- Brun, R. & Carminati, F., GEANT Detector Description and Simulation Tool, CERN Program Library Long Writeup W5013 edition, 1993, CERN, Geneva
- Busso, M., Gallino, R., Lambert, D. L., Travaglio, C., & Smith, V. V., 2001, *ApJ*, 557, 802
- Cowan, J. J., Thielemann, F.-K., & Truran, J. W., 1991, *Phys. Rep.*, 208, 267

- Dietrich, S. S. & Berman, B. L., 1988, *At. Data Nucl. Data Tables*, 38, 199
- ENSDF data base, revision of 15 November, 2001, using NNDC Online Data Service
- Gallino, R., Arlandini, C., Busso, M., Lugaro, M., Travaglio, C., Straniero, O., Chieffi, A., & Limongi, M., 1998, *ApJ*, 497, 388
- Goryachev, A. M. & Zalesnyĭ, G. N., 1978, *IZV. An. KazSSR*, 6, 8
- Gurevich, G. M., Lazareva, L. E., Mazur, V. M., Merkulov, S. Yu., Solodukhov, G. V., & Tyutin, V. A., 1981, *Nucl. Phys.*, A351, 257
- Holmes, J., Woosley, S., Fowler, W., & Zimmerman, B., 1976, *At. Data Nucl. Data Tables*, 18, 305
- Jeukenne, J., Lejeune, A., & Mahaux, C., 1977, *Phys. Rev. C*, 16, 80
- Käppeler F., Gallino, R., Busso, M., Picchio, G., & Raiteri, C. M., 1990, *ApJ*, 354, 630
- Käppeler, F., Jaag, S., Bao, Z. Y., & Reffo, G., 1991, *ApJ*, 366, 605
- Kempisty, T. & Pochwalski, K., 1992, *Nucl. Inst. Meth. A*, 312, 390
- Koehler, P. E., Harvey, J. A., Guber, K. H., Winters, R. R., & Raman, S., *Proc. Int. Conf. on Nuclear Data for Science and Technology*, Tsukuba, Japan, 2001 (in press)
- Lambert, D. L., 1992, *A&A Rev.*, 3, 201
- Lindenberg, K., Neumann, F., Galaviz, D., Hartmann, T., Mohr, P., Vogt, K., Volz, S., & Zilges, A., 2001, *Phys. Rev. C*, 63, 047307
- McCullagh, C. M., Stelts, M. L., & Chrien, R. E., 1981, *Phys. Rev. C*, 23, 1394
- Mengoni, A. & Nakajima, Y., 1994, *J. Nucl. Sci. Tech.*, 31, 151
- Mohr, P., Enders, J., Hartmann, T., Kaiser, H., Schiesser, D., Schmitt, S., Volz, S., Wissel, F., & Zilges, A., 1999, *Nucl. Inst. Meth. A*423, 480
- Mohr, P., Vogt, K., Babilon, M., Enders, J., Hartmann, T., Hutter, C., Rauscher, T., Volz, S., & Zilges, A., 2000a, *Phys. Lett. B*, 488, 127
- Mohr, P., Hutter, C., Vogt, K., Enders, J., Hartmann, T., Volz, S., & Zilges, A., 2000b, *Europ. Phys. J. A*, 7, 45
- Mohr, P., Babilon, M., Enders, J., Hartmann, T., Hutter, C., Vogt, K., Volz, S., & Zilges, A., 2001, *Nucl. Phys. A*688, 82c
- Moldauer, P. A., 1965, *Nucl. Phys.*, 47, 65
- Myers, W. D., Swiatecki, W. J., Kodama, T., El-Jaick, L. J., & Hilf, E. R., 1977, *Phys. Rev. C*, 15, 2032
- Rauscher, T. & Thielemann, F.-K., in *Stellar Evolution, Stellar Explosions, and Galactic Chemical Evolution*, ed. A. Mezzacappa (IOP, Bristol, 1998), p. 483
- Rauscher, T. & Thielemann, F.-K., 2000, *At. Data Nucl. Data Tables*, 75, 1
- Rauscher, T. & Thielemann, F.-K., 2001, *At. Data Nucl. Data Tables*, 79, 47
- Rauscher, T., Thielemann, F.-K., & Kratz, K.-L., 1997, *Phys. Rev. C*, 56, 1613
- Reifarh, R., Arlandini, C., Heil, M., Käppeler, F., Sedyshev, P. V., Mengoni, A., Herman, M., Rauscher, T., Gallino, R., & Travaglio, C. *ApJ* (submitted)
- Richter, A., *Proc. 5<sup>th</sup> European Particle Accelerator Conference*, Barcelona 1996, ed. S. Myers *et al.*, IOP Publishing, Bristol, 1996, p. 110
- Takahashi, K. & Yokoi, K., 1987, *At. Data Nucl. Data Tables*, 36, 375
- Utsunomiya, H., private communication in 2001 and to be published
- Varlamow, V. V., et al., *The Centre for Photonuclear Experiments Data (CDFE) nuclear data bases*, <http://depni.npi.msu.su/cdfe>, Moscow State University, 2001
- Veyssière, A., Beil, H., Bergère, R., Carlos, P., & Leprêtre, A., 1970, *Nucl. Phys. A*159, 561
- Vogt, K., Mohr, P., Babilon, M., Enders, J., Hartmann, T., Hutter, C., Rauscher, T., Volz, S., & Zilges, A., 2001, *Phys. Rev. C*, 63, 055802

- Vogt, K., Mohr, P., Babilon, M., Bayer, W.,  
Hartmann, T., Hutter, C., Rauscher, T.,  
Sonnabend, K., Volz, S., & Zilges, A., 2002,  
Nucl. Phys. A, 707, 216
- Ward, R. A., Newman, M. J., & Clayton, D. D.,  
1976, ApJS, 31, 33
- Winters, R. & Macklin, R., 1981, Phys. Rev. C,  
25, 208

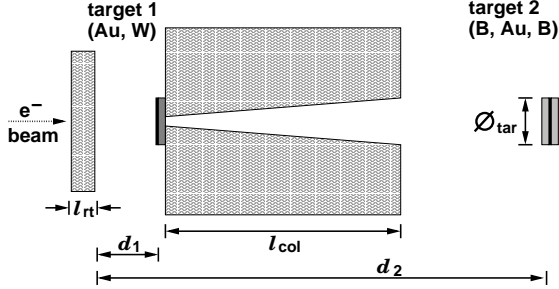


Fig. 1.— Scheme of the photoactivation setup at the S-DALINAC. The radiator target ( $l_{rt} = 1.4$  cm) which generates the photon beam and the collimator ( $l_{col} = 95.5$  cm) are sketched as well as the irradiation positions of our targets ( $d_1 \approx 5$  cm,  $d_2 \approx 150$  cm,  $\varnothing_{tar} = 2$  cm). Note that the lengths are off scale!

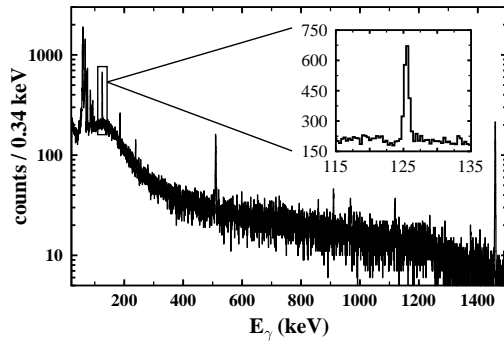


Fig. 2.— Typical  $\gamma$ -ray spectrum of the activated tungsten target. The 125.4 keV line from the weak  $\gamma$ -ray branching in the decay  $^{185}\text{W} \rightarrow ^{185}\text{Re}$  can clearly be identified (see inset). The measuring time for this spectrum was twelve hours.

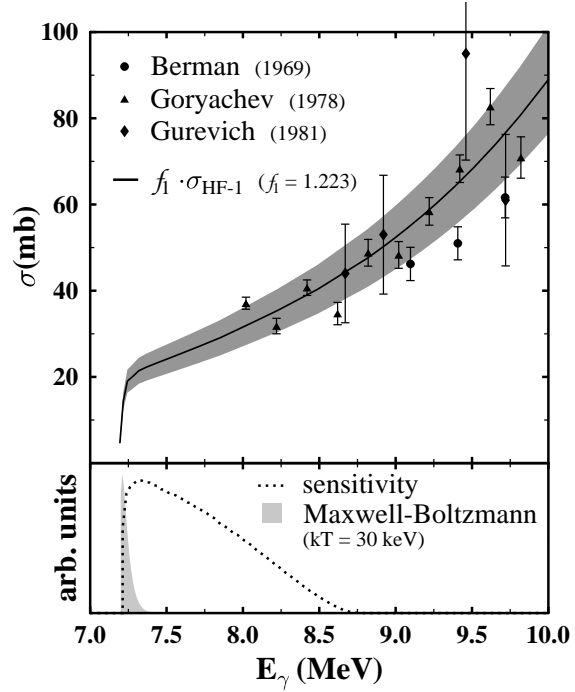


Fig. 3.— Cross section of the  $^{186}\text{W}(\gamma, n)^{185}\text{W}$  reaction. At higher energies data from literature are available (Berman et al. 1969; Goryachev & Zalesnyĭ 1978; Gurevich et al. 1981). The theoretical calculation HF-1 (see Sec. 3), normalized by  $F_1 = 1.223$  (upper part, full line, uncertainties gray shaded) agrees nicely with these data. The sensitive energy range of our new experiment is located close above the  $(\gamma, n)$  threshold (lower part, dotted line). The astrophysically relevant energy range which is defined by a Maxwell-Boltzmann distribution with  $kT = 30$  keV above the threshold at 7194 keV is also shaded (lower part, light gray).

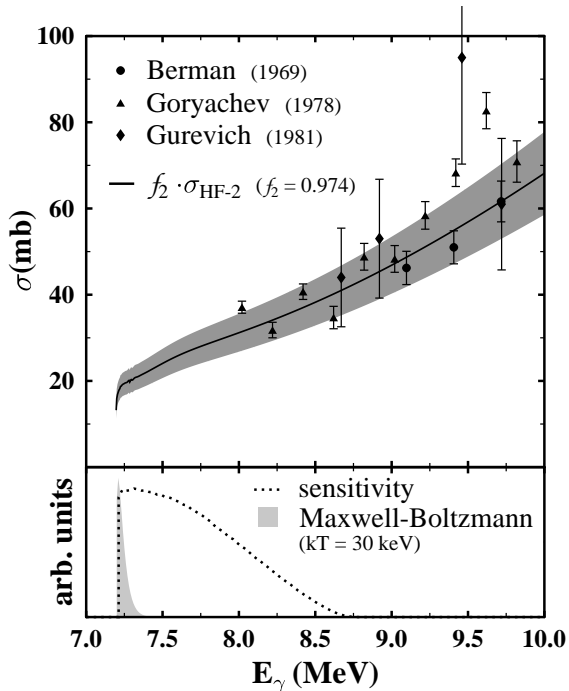


Fig. 4.— Cross section of the  $^{186}\text{W}(\gamma, n)^{185}\text{W}$  reaction. Same as Fig. 3, but with the theoretical calculation HF-2 (see Sec. 3), normalized by  $F_2 = 0.974$  (upper part, full line, uncertainties gray shaded) which again agrees nicely with the available data. The sensitive energy range of our new experiment is located close above the  $(\gamma, n)$  threshold (lower part, dotted line). The astrophysically relevant energy range which is defined by a Maxwell-Boltzmann distribution with  $kT = 30 \text{ keV}$  above the threshold at  $7194 \text{ keV}$  is also shaded (lower part, light gray).

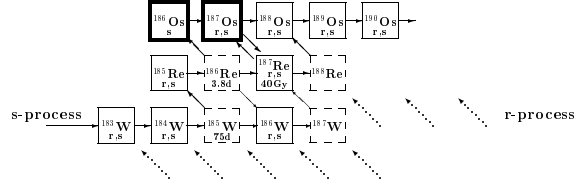


Fig. 5.— The  $s$ -process path in the W-Re-Os mass region. Two branchings occur at  $^{185}\text{W}$  and at  $^{186}\text{Re}$ . Unstable nuclei are marked by dashed boxes (except the quasi-stable  $^{187}\text{Re}$ ). The indicated values are the terrestrial half-lives. Note that the half-life of  $^{187}\text{Re}$  decreases by ten orders of magnitude at stellar temperatures and common densities of the He-intershell while  $^{187}\text{Os}$  becomes unstable (Takahashi & Yokoi 1987).

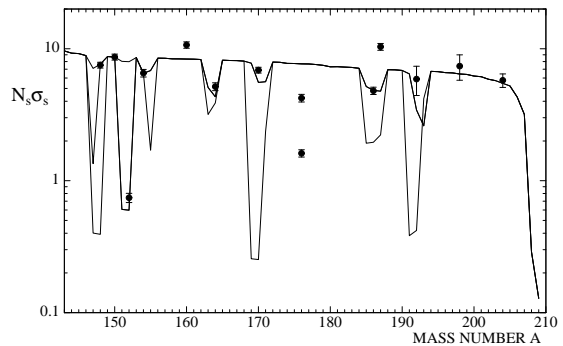


Fig. 6.— The calculated  $N_s\sigma_s$  curve (solid line) shown in the mass range from  $A = 145$  to the termination of the  $s$ -process at  $^{209}\text{Bi}$ . Empirical data are given as solid circles. Important branchings of the  $s$ -process path occur at  $A = 147 - 148$ ,  $151 - 152$ ,  $154 - 155$ ,  $163 - 164$ ,  $169 - 171$ ,  $185 - 187$ , and  $191 - 192$ . The curve is normalized to  $^{150}\text{Sm}$  on the unique path. The data points at  $A = 176$  and  $187$  are not on the curve due to the long lived radioactive decay of  $^{176}\text{Lu}$  and  $^{187}\text{Re}$ .

Table 1: Properties of the tungsten and the gold target which were used during the activation experiment.

Target	Mass (mg)	Nucleus	Abundance (%)	$S_n$ (keV)
tungsten	5847.8(10)	$^{186}\text{W}$	28.6	7194
gold	163.5(5)	$^{197}\text{Au}$	100.0	8071

Table 2: Decay properties of the residual nuclei  $^{185}\text{W}$  and  $^{196}\text{Au}$ .

Nucleus	$T_{1/2}$ (d)	$E_\gamma$ (keV)	$I_\gamma$ (%)
$^{185}\text{W}$	75.1(3)	125.4	0.0192(7)
$^{196}\text{Au}$	6.1669(6)	333.0	22.9(6)
		355.7	87.0(8)
		426.1	6.6(8)

Table 3: Neutron densities in the classical  $s$ -process model from various branchings.

Branch points	$s$ -only isotope	$n_n$ ( $10^8 \text{ cm}^{-3}$ )	Reference
$^{95}\text{Zr}$	$^{96}\text{Mo}$	$4^{+3}_{-2}$	1
$^{147}\text{Nd}/^{147}\text{Pm}/^{148}\text{Pm}$	$^{148}\text{Sm}$	$3.0 \pm 1.1$	1
		$4.9^{+0.6}_{-0.5}$	2
$^{169}\text{Er}/^{170}\text{Tm}$	$^{170}\text{Yb}$	$1.8^{+4.5}_{-0.8}$	1
$^{185}\text{W}/^{186}\text{Re}$	$^{186}\text{Os}$	$4.1^{+1.2}_{-1.1}$	3
$^{185}\text{W}/^{186}\text{Re}$	$^{186}\text{Os}$	$3.8^{+0.9}_{-0.8}$	4
$^{191}\text{Os}/^{192}\text{Ir}$	$^{192}\text{Pt}$	$0.7^{+0.05}_{-0.02}$	5

REFERENCES.—(1) Käppeler et al. (1990); (2) Reifarth et al. (2002); (3) Käppeler et al. (1991); (4) this work; (5) Koehler et al. (2001).